Sensors & Actuators: B. Chemical 451 (2026) 139348

Contents lists available at ScienceDirect

Sensors and Actuators: B. Chemical

journal homepage: www.elsevier.com/locate/snb

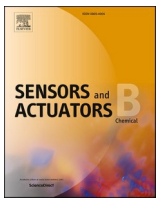

Visualization of tetracycline induced pancreatitis by chymotrypsin-activated near-infrared fluorogenic probe

Wanwei Zhang [a], Mo Ma [a,b], Chen Zhao [a], Pinyi Ma [a], Daqian Song [a], Ying Sun [a,*]

[a] College of Chemistry, Jilin Province Research Center for Engineering and Technology of Spectral Analytical Instruments, Jilin University, Qianjin Street 2699, Changchun 130012, China
[b] School of Pharmacy, Jilin University, Qianjin Street 2699, Changchun 130012, China

ARTICLE INFO

Keywords:
Fluorescence probe
Chymotrypsin
Drug induced pancreatitis
Tetracycline

ABSTRACT

Acute pancreatitis (AP) is a common digestive system disease with severe symptoms. Its causes are diverse, including drug induced pancreatitis (DIP) on the rise in recent years. Antibiotic drugs such as tetracycline, which induced AP has received considerable attention. Tetracycline disrupts pancreatic cell apoptosis, proliferation and activate inflammatory signaling pathways. Chymotrypsin (CHT) is the main digestive protease in the pancreas and is crucial for the development of pancreatitis. Thus, there is an urgent need to develop a practical and efficient approach for real-time tracking of CHT secretion from pancreatic cells under drug-induced pancreatitis (DIP) conditions. To address this challenge, we report the rational design and synthesis of a near-infrared fluorescent probe, termed HNTC-DIP, for highly accurate monitoring of CHT dynamics in a tetracycline-induced pancreatitis model. The probe rapidly detects CHT within 5 min through enzymatic cleavage of its ester bonds, which restores the intramolecular charge transfer (ICT) process. The fluorescence intensity shows a 14–15-fold enhancement. In addition, it has been utilized effectively to bioimage and evaluate endogenous CHT variations in DIP models (tetracycline -induced pancreatitis model). HNTC-DIP can serve as a reliable and suitable tool for accurately visualizing DIP damage for the first time and these applications also demonstrate the potential in the risk assessment of clinical application for antibiotic drugs.

1. Introduction

AP is an inflammatory disorder of the pancreas characterized by severe tissue damage and necrosis [1,2]. The incidence of AP continues to rise, posing a significant healthcare and socioeconomic burden [3,4]. Gallstones and excessive alcohol consumption are the primary risk factors, while approximately 15–25 % of cases are attributed to other causes such as drug induced [5–7]. In recent years, more attentions have been paid to DIP [8]. Notably, tetracycline-associated DIP has become a focus of clinical concern [9–11]. The first reported association between tetracycline and AP dates back to the 1960s in women receiving intravenous therapy for fatty liver disease [12]. Subsequently, large-scale pharmacoepidemiologic studies have demonstrated that tetracycline users (defined as individuals with prescriptions filled within 0–30 days prior to the index date of pancreatitis diagnosis) has 60 % increased risk of AP [12]. Through an integrated approach combining network toxicology and molecular docking, researchers such as Lei et al. have elucidated tetracycline's toxic pathways in AP. Tetracycline may trigger inflammation, apoptosis, and metabolic dysregulation in pancreatic cells by modulating core targets such as TP53, TNF, and AKT1, as well as related signaling pathways (e.g., PI3K-Akt, MAPK), ultimately leading to AP [13]. Scheme 1

Pancreatic lipase, trypsin, and CHT are all enzymes specifically expressed in the pancreas. Fan et al. analyzed pancreatic lipase using a fluorescence probe for early diagnosis of severe acute pancreatitis [14]. Ning et al. detected trypsin for screening trypsin inhibitor drugs [15]. CHT, as a crucial digestive protease in the pancreas, plays a pivotal role in the pathogenesis of pancreatitis [16]. It not only participates in food digestion, but also regulates trypsin activity through the degradation of trypsinogen, maintaining pancreatic homeostasis [17–21]. Currently, several biochemical methods exist for CHT detection, including fiber-based interferometry, mass spectrometry (MS), high-performance liquid chromatography (HPLC), and enzyme-linked immunosorbent assay (ELISA) [22–24]. However, most of these techniques suffer from limitations such as high cost and complex procedures. In contrast, fluorescent probes offer distinct advantages including excellent

* Corresponding author.
E-mail address: yingsun@jlu.edu.cn (Y. Sun).

https://doi.org/10.1016/j.snb.2025.139348
Received 19 October 2025; Received in revised form 1 December 2025; Accepted 16 December 2025
Available online 16 December 2025

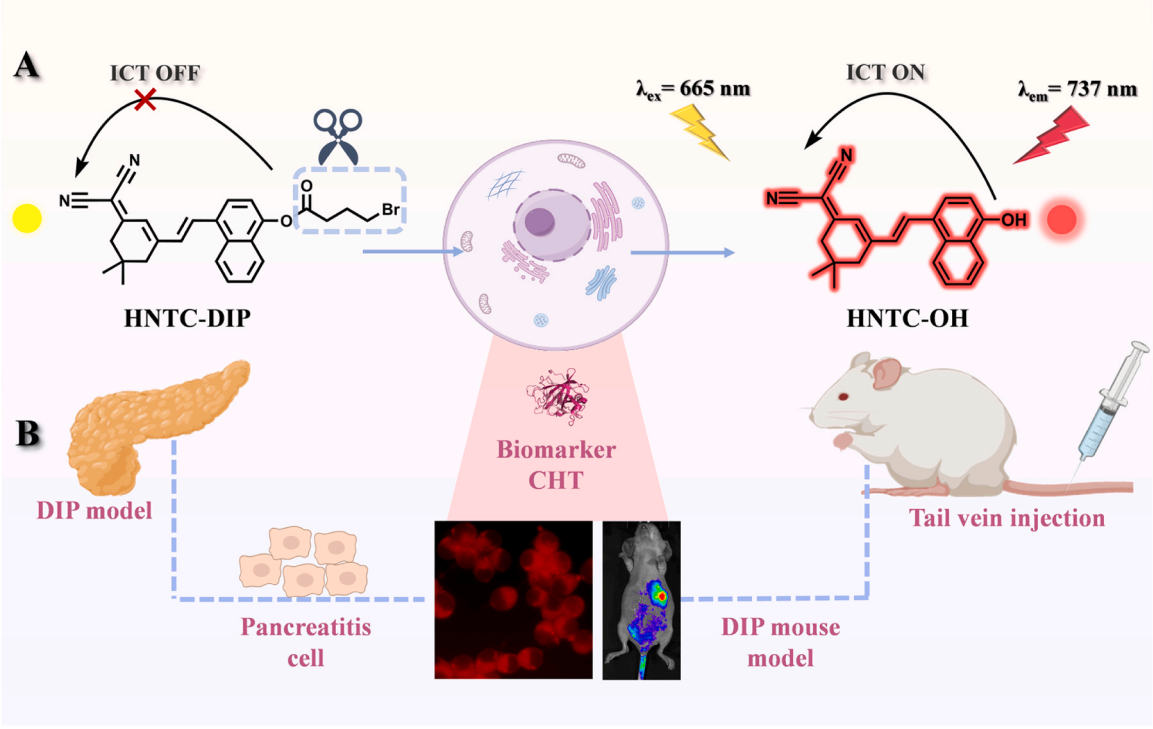

Scheme 1. (A) Response mechanism of HNTC-DIP with CHT. (B) NIR fluorescence imaging of CHT in DIP.

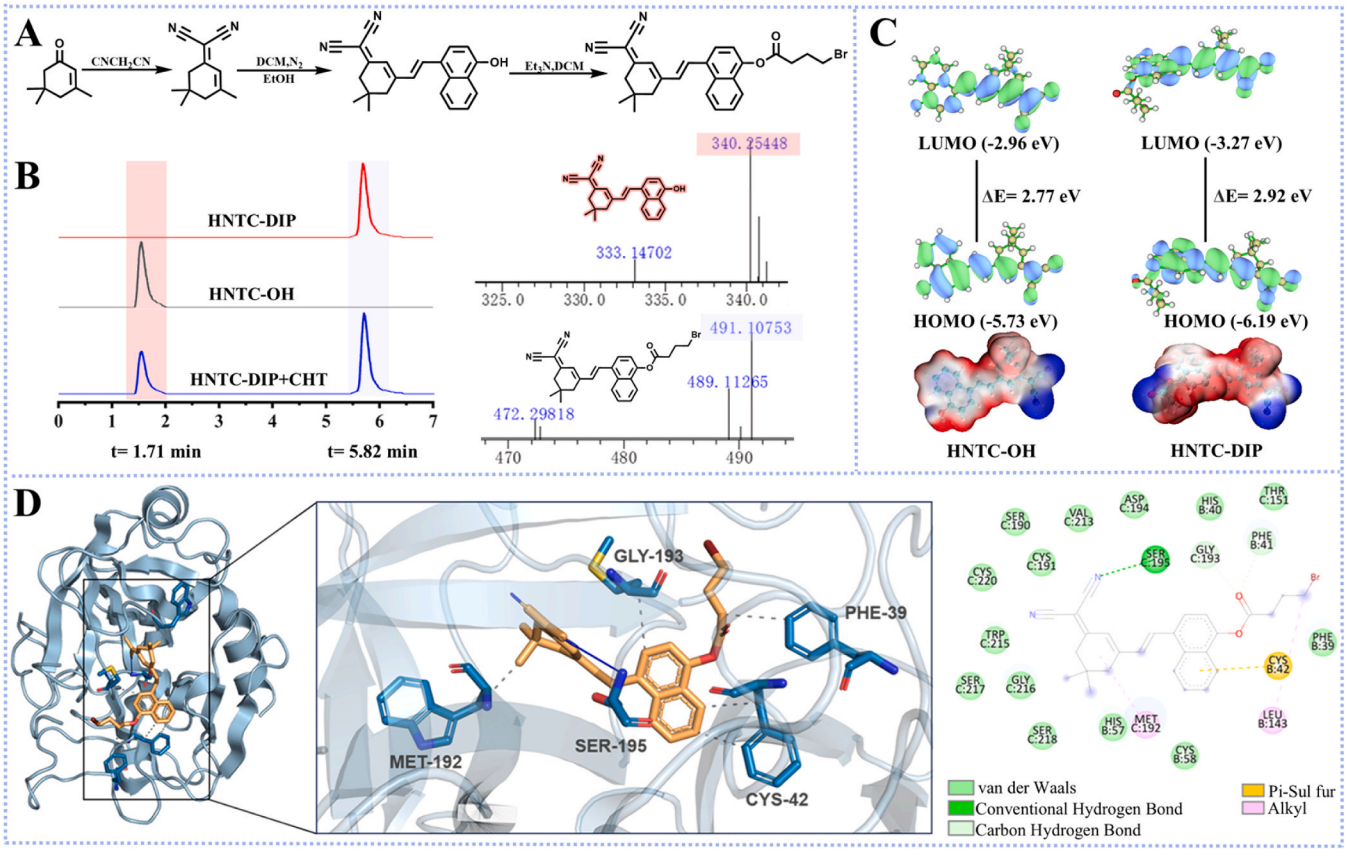

Fig. 1. Recognition and response mechanism of HNTC-DIP to CHT. (A) Synthetic route of HNTC-DIP. (B) LC-MS validation of the response mechanism of HNTC-DIP toward CHT. (C) Results of density functional theory (DFT) computations for HNTC-OH and HNTC-DIP. (D) Molecular docking simulation of the interaction between HNTC-DIP and CHT was performed using Autodock Vina.

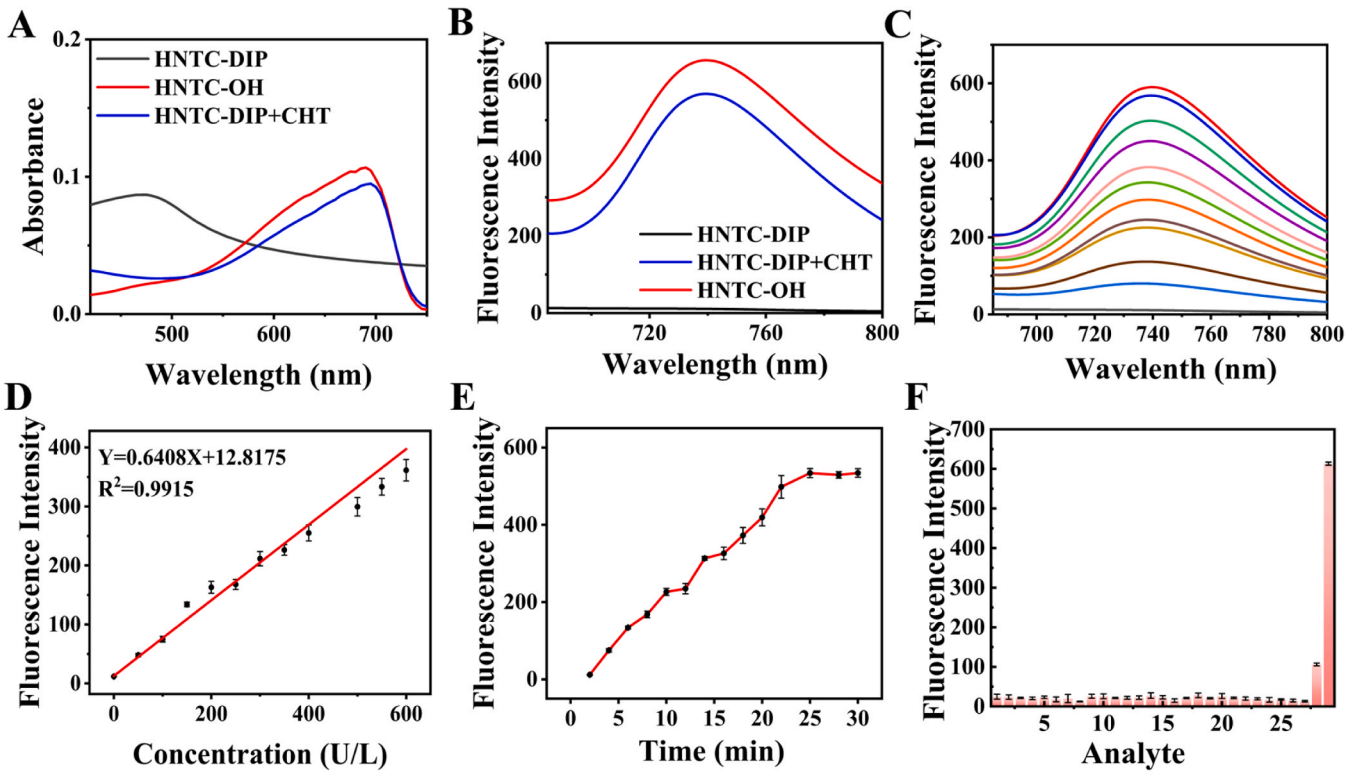

Fig. 2. Spectroscopic properties and selectivity of HNTC-DIP. (A) Absorption spectral changes of HNTC-DIP (1 mM) upon reaction with 1 mM CHT. (B) Fluorescence spectral responses of HNTC-DIP following treatment with CHT. (C) Spectral variations of HNTC-DIP (10 μM) titrated with increasing concentrations of CHT (0–800 U/L). (D) Linear correlation of HNTC-DIP (10 μM) and CHT (0–600 U/L). (E) Time-dependent fluorescence response of HNTC-DIP to CHT (800 U/L). (F) Fluorescence intensity of HNTC -DIP (10 μM). (Number 1–29: probe only, Cu^{2+}, Zn^{2+}, K^{+}, Ca^{2+}, Na^{+}, Mg^{2+}, F^{-}, Cl^{-}, Br^{-}, HCO_3^{-}, HS^{-}, CO_3^{2-}, SO_3^{2-}, PO_4^{3-}, GSH, Cys, Hcy, LAP, ALP, AChE, BChE, CES2, Try, NE, $ONOO^{-}$, O_2^{-}, PL, CHT). (mean ± SD, n = 3).

biocompatibility, non-invasiveness, high sensitivity, and real-time visualization capabilities, enabling in situ monitoring of CHT activity [25–28]. Notably, no fluorescent probes have been reported for detecting CHT in DIP models to date [29–32]. To address this gap, we rationally designed and developed a novel near-infrared (NIR) fluorescent probe, HNTC-DIP, for precise monitoring of CHT fluctuations in tetracycline-induced pancreatitis.

Here we report a near-infrared fluorescent probe HNTC-DIP based on dicyano-isoflurone for CHT activity [33]. Tetrabromobutyryl chloride group of HNTC-DIP serves as a specific recognition unit for CHT, enabling its selective identification. Following this recognition, HNTC-DIP binds to CHT via hydrogen bonding interactions. Compared to existing probes, HNTC-DIP exhibits specific responses to CHT in vitro, with the characteristics of rapid imaging and near-infrared light emission [34–36]. HNTC-DIP also has excellent photostability, selectivity, biological safety and low cytotoxicity, and can quantitatively detect CHT within the range of 0–1600 U/L. We studied the sensing mechanism of HNTC-DIP using molecular docking simulations, liquid chromatography-high resolution mass spectrometry (LC-HRMS), etc. The mechanism of interaction between HNTC-DIP and CHT is that CHT breaks the ester bond, allowing HNTC-DIP to return to the fluorescent group HNTC-OH. Naphthalene serves as an excellent conjugated bridge for designing fluorophores with red-shifted emission profiles. The photophysical characteristics of such systems are critically influenced by the nature of the π-bridge and the spatial arrangement between donor (D) and acceptor (A) units. The naphthalene-linked fluorescent group has a longer emission wavelength than previous benzene-linked fluorescent groups [37]. The red shift of HNTC-OH in fluorescence was confirmed by experimental measurement and theoretical calculation, and its strong ICT process was confirmed. In DIP cells, HNTC-DIP was successfully activated and real-time monitored CHT in DIP for the first time. Subsequently, it was injected into the DIP mice model via the tail vein, and could accurately perform real-time fluorescence imaging of the pancreas. This confirmed that HNTC-DIP has the ability to image the fluctuation of CHT during the process of DIP. Thus, HNTC-DIP successfully visualized CHT fluctuations during DIP progression, providing clinicians and patients with a more intuitive tool for recognizing tetracycline-induced pancreatitis.

2. Experimental procedure

2.1. General information

All reagents and instruments used in this study are detailed in the Supporting Information. Fluorophore HNTC-OH and compound 1 were prepared and characterized according to previously reported procedures, with their structural confirmation provided in Figures S1–S4.

2.2. Synthesis of HNTC-DIP

HNTC-OH (340 mg, 1 mmol) was dissolved in dichloromethane (10 mL), cooled in an ice bath for 10 min, followed by dropwise addition of triethylamine (101 mg, 1 mmol) under continuous stirring at 0 °C for an additional 10 min. Then 4-bromobutanoyl chloride (185.4 mg, 1 mmol) was slowly added and stirred at room temperature for 30 min. The yellow product HNTC-DIP (259 mg, 53 %) was obtained by using dichloromethane/ethyl acetate (v/v, 80:1) as eluent. ^{1}H NMR (300 MHz, $CDCl_3$) δ 8.19 – 8.10 (m, 1 H), 8.02 – 7.87 (m, 1 H), 7.85 – 7.72 (m, 2 H), 7.68 – 7.53 (m, 2 H), 7.31 (d, J = 8.1 Hz, 1 H), 7.02 (d, J = 15.8 Hz, 1 H), 6.87 (s, 1 H), 3.60 (t, J = 6.3 Hz, 2 H), 2.99 (t, J = 7.2 Hz, 2 H), 2.59 (d, J = 14.3 Hz, 4 H), 2.46 – 2.31 (m, 2 H), 1.12 (s, 6 H) ^{13}C NMR (151 MHz, $CDCl_3$) δ 170.99, 170.95, 169.27, 169.17,

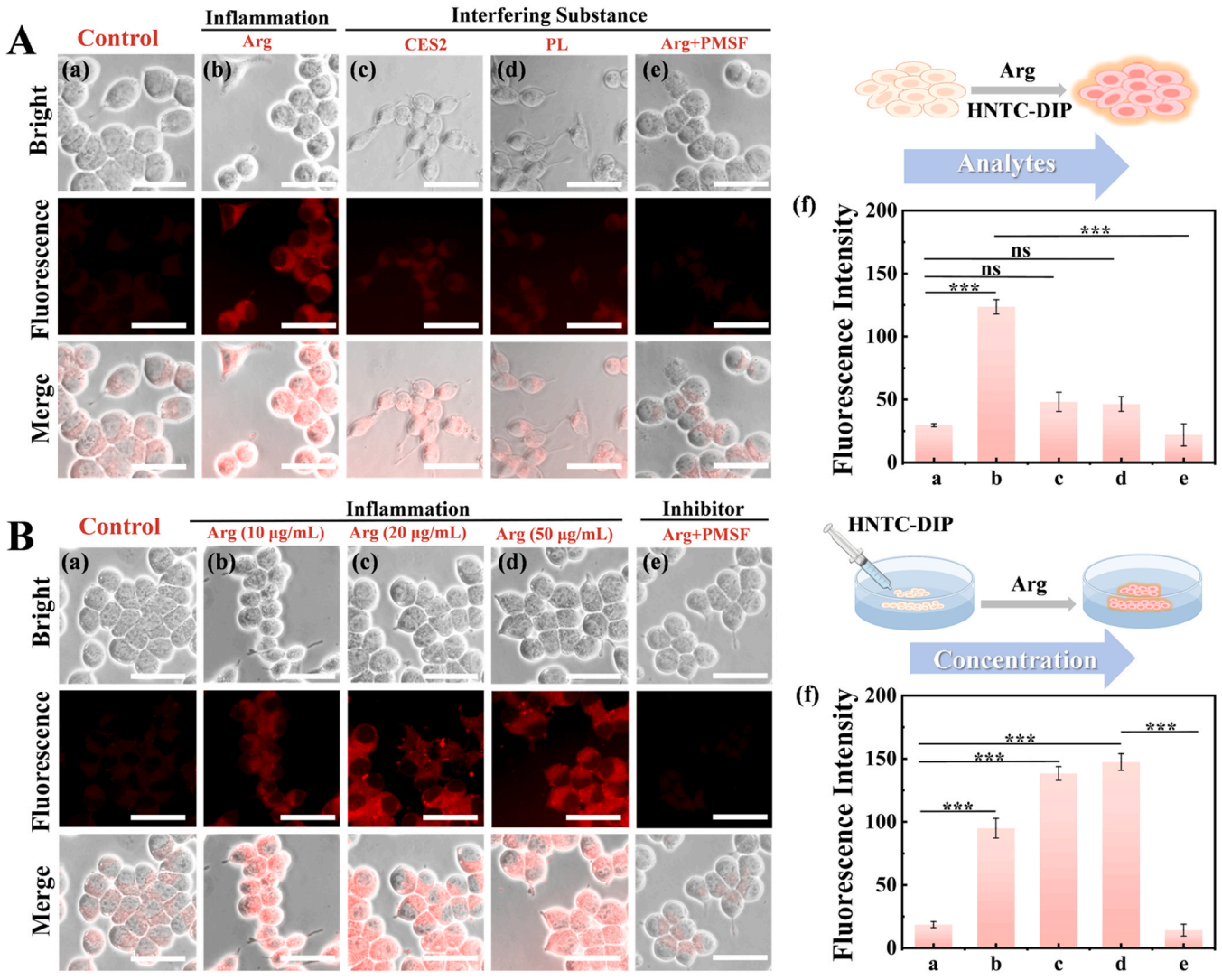

Fig. 3. Fluorescence imaging of living cells subjected to various pretreatment conditions in vitro. (A) (a) AR42J cells incubated with 10 μM HNTC-DIP alone for 0.5 h; (b) AR42J cells pretreated with 20 μg/mL Arg for 12 h; (c) AR42J cells pretreated with 100 μM CES2 for 12 h; (d) AR42J cells pretreated with 100 μM PL for 12 h; (e) AR42J cells pretreated with 50 μg/mL Arg and 300 μM PMSF for 12 h. (B) (a) AR42J cells incubated with 10 μM HNTC-DIP alone for 0.5 h; (b) AR42J cells pretreated with 10 μg/mL Arg for 12 h, followed by incubation with 10 μM HNTC-DIP for 0.5 h; (c) AR42J cells pretreated with 20 μg/mL Arg for 12 h, followed by incubation with 10 μM HNTC-DIP for 0.5 h; (d) AR42J cells pretreated with 50 μg/mL Arg for 10 h, followed by incubation with 12 μM HNTC-DIP for 0.5 h; (e) AR42J cells pretreated with 50 μg/mL Arg, then cotreated with 300 μM PMSF for 0.5 h, and finally stained with 10 μM HNTC-DIP for 0.5 h. Scale bar: 200μm. (*P ≤ 0.05; ** P ≤ 0.01; *** P ≤ 0.001; **** P ≤ 0.0001, data analyses were performed on independent samples with equal variances; mean ± SD; n = 3).

154.76, 153.53, 147.70, 146.91, 135.97, 133.16, 132.84, 132.81, 132.70, 132.32, 132.21, 131.99, 131.80, 131.26, 127.35, 127.26, 127.17, 127.00, 126.98, 126.87, 126.75, 126.73, 126.29, 125.27, 125.21, 125.20, 124.49, 124.42, 124.05, 123.95, 123.48, 123.39, 122.15, 122.00, 121.79, 118.25, 118.18, 117.47, 113.43, 113.14, 112.65, 112.25, 79.63, 79.23, 43.05, 42.60, 42.38, 42.33, 39.40, 32.52, 32.50, 32.11, 29.71, 28.10, 27.58, 27.56, 27.39, 13.05, 9.55, 9.47. HR-MS (m/z): Calculated for $[C_{27}H_{26}BrN_2O_2]^+$: 491.1152, found: 491.1075. (Figures S5, S6 and S7).

2.3. Spectrophotometric measurement

For spectral characterization, a solution of HNTC-DIP (10.0 μM) in phosphate-buffered saline (PBS) with DMSO was prepared and incubated with CHT at 37 °C for 40 min.

2.4. Fluorescence imaging and cell culture

Full details of the cell culture procedures are provided in the Supporting Information. AR42J cells were maintained in Dulbecco's Modified Eagle Medium (DMEM) supplemented with 10 % fetal bovine serum (FBS) under standard conditions.

2.5. Fluorescence imaging in AP and DIP models of mice

Following a one-week adaptation period, mice were randomly assigned to three experimental groups: (1) the control group, administered physiological saline; (2) the L-arginine (Arg)-induced model group, receiving three intraperitoneal injections of Arg within 12 h; and (3) the tetracycline hydrochloride (TCH)-induced model group, receiving three intraperitoneal injections of TCH within 12 h. A detailed experimental protocol is provided in the Supporting Information.

3. Results and discussion

3.1. Synthesis route and response mechanism of HNTC-DIP

The detailed synthesis of HNTC-DIP is shown in Fig. 1A. The reaction

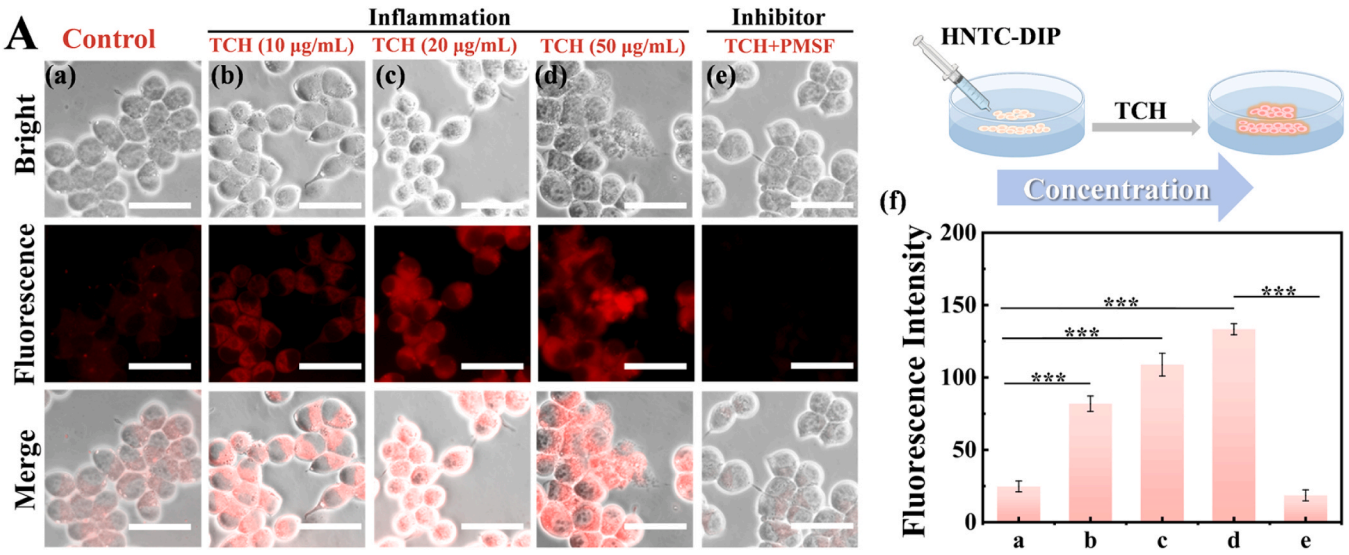

Fig. 4. (A) (a) AR42J cells following 0.5 h treatment with 10 μM HNTC-DIP; (b) AR42J cells after 12 h treatment with 10 μg/mL TCH, then treated with 10 μM HNTC-DIP for 0.5 h; (c) AR42J cells after 12 h treatment with 20 μg/mL TCH, then treated with 10 μM HNTC-DIP for 0.5 h; (d) AR42J cells after 12 h treatment with 50 μg/mL TCH, then treated with 10 μM HNTC-DIP for 0.5 h; (e) AR42J cells were first pretreated with 50 μg/mL TCH and then co-incubated with PMSF (300 μM) for 0.5 h, followed by staining with 10 μM HNTC-DIP for an additional 0.5 h. Scale bar: 200 μm. (*P ≤ 0.05; ** P ≤ 0.01; *** P ≤ 0.001; **** P ≤ 0.0001, data analyses were performed on independent samples with equal variances; mean ± SD; n = 3).

of HNTC-DIP to CHT was used for LC-MS analysis to further confirm and elucidate the specific and rapid response mechanism (Fig. 1B). Electrostatic potential mapping of HNTC-DIP and HNTC-OH clearly demonstrated an intramolecular charge transfer (ICT) feature with pronounced electron push-pull properties in HNTC-OH. This ICT effect, facilitated by its D–π–A configuration, ultimately induced intense fluorescence emission (Fig. 1C). Furthermore, the recognition moiety 4-bromobutyrylcan effectively quenches the fluorescence of HNTC-OH by disrupting its ICT process [38,39]. The CHT-specific recognition mechanism of HNTC-DIP was further elucidated [40,41]. Enzymatic hydrolysis of the ester bond between HNTC-OH and the 4-bromobutyryl recognition group by CHT restored the ICT process, leading to significant fluorescence recovery (Fig. 1D). Molecular docking simulations revealed a binding energy of −7.7 kcal/mol between HNTC-DIP and CHT, indicating strong binding affinity between the probe and the target enzyme.

3.2. Spectral response and probe selectivity

HNTC-DIP itself shows a strong absorption maximum at 490 nm. After treatment with CHT, the absorption peak redshifted to approximately 690 nm (Fig. 2A), along with a significant 43-fold fluorescence increase at 737 nm (Fig. 2B). The fluorescence titration results demonstrated that fluorescence enhancement of the reaction system exhibited good linearity with an equation of Y= 0.6408X+ 12.8175, R^2= 0.9915 in the concentration range of 0–600 U/L for CHT (Fig. 2C and 2D). The detection limit was found to be 0.51 U/L. As shown in Fig. 2E, upon introducing CHT (600 U/L) to HNTC-DIP solution, there was a rapid enhancement in fluorescence intensity at 727 nm, with the curve leveling off after 25 min. To study the specific selectivity of HNTC-DIP for CHT, we examined the impact of various analytes. As depicted in Fig. 2F, HNTC-DIP displayed high selectivity toward cations (Cu^{2+}, Zn^{2+}, K^+, Na^+, Ca^{2+}, and Mg^{2+}), anions (Br^-, F^-, Cl^-, HCO_3^-, HS^-, CO_3^{2-}, SO_3^{2-}, and PO_4^{3-}), reactive sulfur (GSH, Cys, and Hcy), biological enzymes (Leucine Aminopeptidase, Alkaline Phosphatase, Acetylcholinesterase, Butyrylcholinesterase, Carboxylesterase 2, Trypsin, Neutrophil Elastase and Pancreatic Lipase) and RNS/ROS ($ONOO^-$, O_2^-). These analytes exhibited minimal reactivity, indicating the exceptional selectivity of HNTC-DIP for CHT and its suitability for use in complex biological environments. As demonstrated in Figures S8 and S9, the fluorescence intensity of HNTC-DIP alone remains largely stable across a pH range of 5.6–9.1 and temperatures between 25 and 42 °C. After reaction with CHT, maximum fluorescence enhancement was observed at pH 7.4 and 37 °C, indicating optimal performance of HNTC-DIP under physiologically relevant conditions. Moreover, it displayed an excellent photostability under the irradiation of a xenon lamp (Figure S10). Therefore, HNTC-DIP can serve as an effective probe for selective detection of CHT under complex physiological conditions. Subsequently, the enzyme kinetics between HNTC-DIP and CHT was investigated. Michaelis−Menten diagram and the Lineweaver−Burk plot are depicted in Figure S11. The catalytic constant (K_{cat}/K_m) was calculated as 91.419 $M^{-1}min^{-1}$.

3.3. Fluorescence imaging of endogenous CHT in living cells

Inspired by the excellent performance in vitro, we evaluated the potential of HNTC-DIP to monitor endogenous CHT in living cells. As shown in Figures S12 and S13, the hemolysis test indicated the excellent biocompatibility and more than 85 % AR42J cells survived even at 10 mM HNTC-DIP, indicating that the cytotoxicity of HNTC-DIP to living cells was negligible. The capacity of HNTC-DIP to detect endogenous CHT was evaluated in AR42J cells that stimulated with Arg, a commonly used agentia to trigger intracellular inflammation. After 30 min of co-incubation with HNTC-DIP, the cells reached a plateau in fluorescence intensity, indicating signal stabilization (Figure S14). As depicted in Fig. 3A, AR42J cells treated with HNTC-DIP showed fluorescence weakly, which indicates a relatively low CHT level under normal conditions. Following 24 h Arg stimulation, we observed a 6.2-fold enhancement in fluorescence intensity. Meanwhile, intracellular fluorescence decreased in the presence of phenyl methane sulfonyl fluoride (PMSF), a scavenger of CHT, implying the specificity of HNTC-DIP in monitoring cellular CHT fluctuations. In CES2 treated or PL treated cells, the fluorescence fluctuations showed no significant variations. These findings affirm the capacity of HNTC-DIP to selectively detect CHT in AR42J cells. As illustrated in Fig. 3B, upon the addition of varying concentrations of Arg followed by a 30 min incubation period, a progressive increase in red fluorescence intensity in AR42J cells was observed. Collectively, these results proved the capability of HNTC-DIP

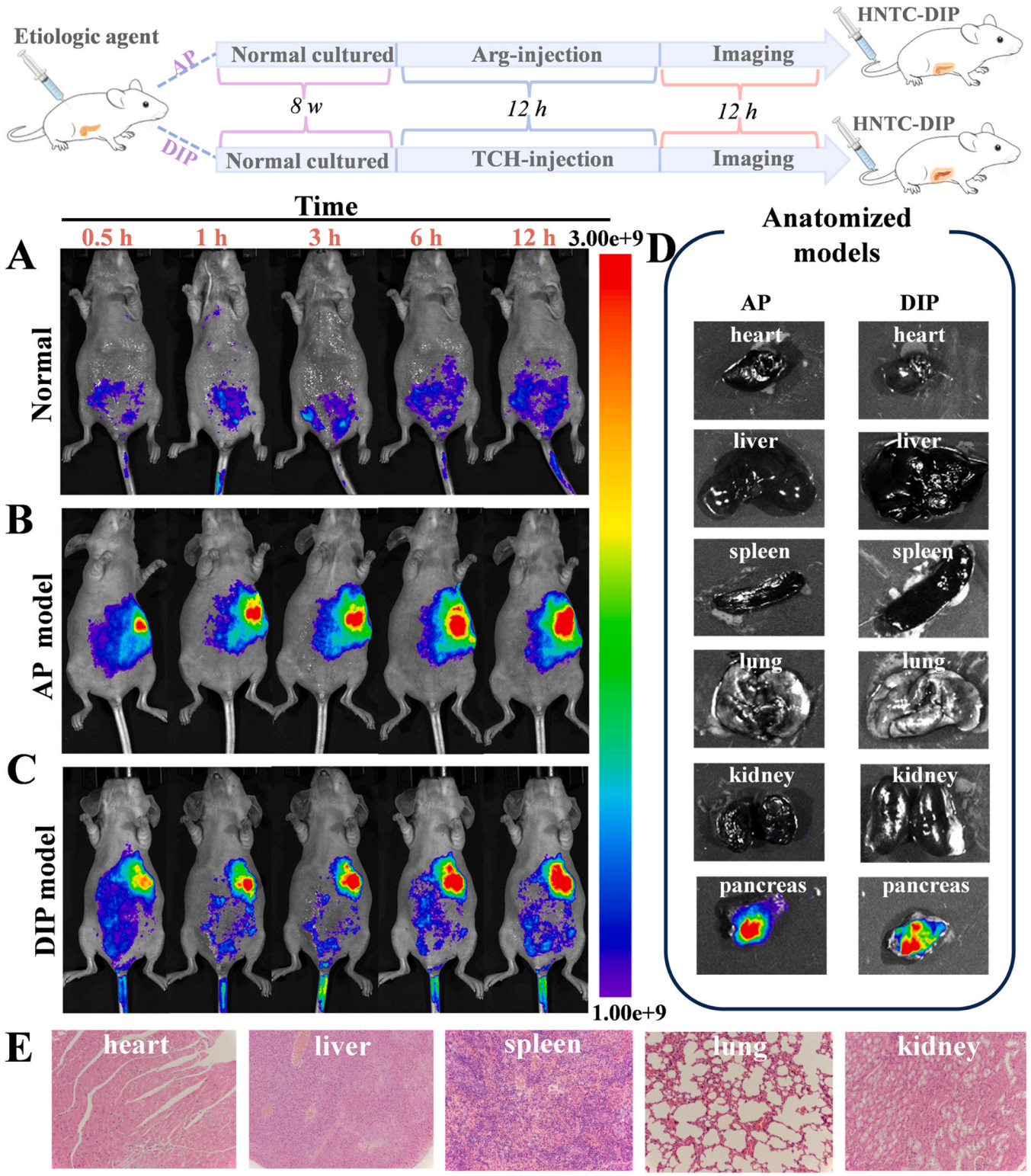

Fig. 5. In vivo fluorescence imaging in mice and major internal organs. (A) Normal mouse after tail injection of HNTC-DIP (200 μM, 50 μL). (B) AP mouse after tail injection of HNTC-DIP (200 μM, 50 μL). (C) DIP mouse after tail injection of HNTC-DIP (200 μM, 50 μL). (D) Ex vivo fluorescence imaging of major organs of AP and DIP model mice. (E) Histopathological analysis of mouse organ sections by H&E staining (20 ×magnification).

to fluorescently visualize CHT in AP cells.

Based on these promising results, we next evaluated the capability of HNTC-DIP to monitor CHT in living pancreatic cells under tetracycline-induced condition. Tetracycline, a widely used antibiotic, has been documented to induce AP. As depicted in Fig. 4, AR42J cells exhibited only weak fluorescence after 30 min of incubation with HNTC-DIP alone. Then, AR42J cells were first pre-incubated with TCH (10–50 μg/mL) for 24 h and then treated with HNTC-DIP for 30 min; this protocol resulted in bright fluorescence showing dose-dependent enhancement. Notably, a 5.2-fold increase in fluorescence intensity was achieved following treatment with 50 μg/mL TCH. The fluorescence is significantly reduced by the pretreatment with PMSF, a known

scavenger of CHT. In short, these observations indicate that HNTC-DIP is a promising probe for the detection of increased endogenous CHT level which is closely related to the DIP process in living AR42J cells.

3.4. Fluorescence imaging of endogenous CHT in AP and DIP models

We next investigated the suitability of HNTC-DIP for in vivo AP imaging by applying it to the AP mice. AP model was established using Arg induction according to previously described methods [42,43]. We initially selected control mice and model mice, then administered HNTC-DIP (200 μM, 50 μL) injection via the tail vein. As shown in Figs. 5A and 5B, the pancreatic fluorescence intensity of the AP mice rose significantly with the model time expanding. Collectively, these results proved the capability of HNTC-DIP to fluorescently visualize CHT in AP mice model. Afterwards, we applied probe HNTC-DIP to trace the endogenous CHT level DIP model mice. As demonstrated in Fig. 5C, intact mice treated with TCH showed significantly enhanced fluorescence, suggesting elevated CHT levels in DIP. Based on these promising results, we next investigated whether HNTC-DIP could be applied for imaging at the whole-organ level. Fluorescence signals from various organs were captured and analyzed after dissecting the mice (Fig. 5D). Interestingly, increased fluorescence signals in the pancreas region were observed in AP and DIP mice. No signs of toxicity were detected in major organs via H&E staining (Fig. 5E) after the administration of HNTC-DIP. Based on the in vivo experiments, HNTC-DIP has been demonstrated to effectively visualize the dynamic changes of CHT in DIP mice models.

4. Conclusion

In summary, we designed and synthesized HNTC-DIP, a NIR fluorescent probe, for the specific detection and in vivo imaging of CHT activity in both AP and DIP mouse models. The probe recovers fluorescence signal by restoration of ICT process through cleavage of ester bonds. Spectroscopic assays revealed that HNTC-DIP responds to CHT within 5 min, yielding a 14–15 fold enhancement in fluorescence intensity. To our knowledge, HNTC-DIP represents the first NIR fluorescent probe capable of visualizing CHT in DIP models. It is found that CHT upregulate in AP and DIP, revealing its importance in pancreas function and its potential value in pancreas diagnosis and therapy. This study alerts physicians to be vigilant about the risk of pancreatitis when prescribing tetracycline, providing new visual evidence for the rational clinical use of tetracycline. It also demonstrates the potential in the clinical application of antibiotic risk assessment. HNTC-DIP may serve as a promising tool for research on CHT associate diseases.

CRediT authorship contribution statement

Pinyi Ma: Funding acquisition, Conceptualization. **Chen Zhao:** Visualization, Investigation. **Ying Sun:** Resources, Project administration, Data curation. **Daqian Song:** Investigation, Funding acquisition. **Mo Ma:** Investigation, Formal analysis. **Wanwei Zhang:** Writing – original draft, Investigation, Formal analysis, Data curation, Conceptualization.

Declaration of Competing Interest

The authors declare that they have no known competing financial interests or personal relationships that could have appeared to influence the work reported in this paper.

Acknowledgment

This work was supported by the National Natural Science Foundation of China (22074052 and 22004046) and the Science and Technology Developing Foundation of Jilin Province of China (20230101033JC).

Appendix A. Supporting information

Supplementary data associated with this article can be found in the online version at doi:10.1016/j.snb.2025.139348.

Data availability

Data will be made available on request.

References

[1] C. Zhang, G. Li, T. Lu, L. Liu, Y. Sui, R. Bai, et al., The interaction of microbiome and pancreas in acute pancreatitis, Biomolecules 14 (2024) 59.
[2] S. Tenner, S.S. Vege, S.G. Sheth, B. Sauer, A. Yang, D.L. Conwell, et al., American college of gastroenterology guidelines: management of acute pancreatitis, Am. J. Gastroenterol. 119 (2024) 419–437.
[3] P.G. Lankisch, M. Apte, P.A. Banks, Acute pancreatitis, Lancet 386 (2015) 85–96.
[4] M.S. Petrov, D. Yadav, Global epidemiology and holistic prevention of pancreatitis, Nat. Rev. Gastroenterol. Hepatol. 16 (2019) 175–184.
[5] M. Runzi, P. Layer, Drug-associated pancreatitis: facts and fiction, Pancreas 13 (1996) 100–109.
[6] C.D. Trivedi, C.S. Pitchumoni, Drug-induced pancreatitis - an update, J. Clin. Gastroenterol. 39 (2005) 709–716.
[7] N. Badalov, R. Baradarian, K. Iswara, J. Li, W. Steinberg, S. Tenner, Drug-induced acute pancreatitis: an evidence-based review, Clin. Gastroenterol. Hepatol. 5 (2007) 648–661.
[8] A.R. Balani, J.H. Grendell, Drug-induced pancreatitis incidence, management and prevention, Drug Saf. 31 (2008) 823–837.
[9] D.P. Nicolau, D.E. Mengedoht, J.J. Kline, Tetracycline-induced pancreatitis, Am. J. Gastroenterol. 86 (1991) 1669–1671.
[10] M.F. Elmore, J.D. Rogge, Tetracycline-induced pancreatitis, Gastroenterology 81 (1981) 1134–1136.
[11] Acute, pancreatitis risk higher in current tetracycline users, Nat. Rev. Gastroenterol. Hepatol. 8 (2011) 658–6518.
[12] R. Ljung, J. Lagergren, T.S. Bexelius, F. Mattsson, M. Lindblad, Increased risk of acute pancreatitis among tetracycline users in a swedish population-based case–control study, Gut 61 (2012) 873–876.
[13] H. Lei, Y. Wu, W. Ma, J. Yao, P. Zhang, Y. Tian, et al., Network toxicology and molecular docking analysis of tetracycline-induced acute pancreatitis: unveiling core mechanisms and targets, Toxics 12 (2024) 929.
[14] H.W. Fan, N. Fang, B.B. Yang, H. Xian, Z. Li, Fluorescence lifetime imaging of human pancreatic lipase activity using a novel probe for early diagnosis of severe acute pancreatitis, Spectrochim. Acta A Mol. Biomol. Spectrosc. 326 (2025) 125171.
[15] J.Y. Ning, X.Y. Bao, H.T. Chen, Z.L. Yan, L. Ding, C. Shu, Dual-mode detection of trypsin and screening of trypsin inhibitors on the basis of a colorimetric/fluorescence sensing probe, Anal. Chem. 97 (2025) 10494–10501.
[16] X. Jin, Q. Wang, T. Xie, S.-T. Xu, D.-A. Chen, G.-Y. Cao, et al., Dual-locked chemiluminescent probe enables precise imaging and timely diagnosis of colitis via chymotrypsin/vanin-1 cascade activation, Anal. Chem. 96 (2024) 18635–18646.
[17] J. Zhou, M. Sahin-Tóth, Chymotrypsin c mutations in chronic pancreatitis, J. Gastroenterol. Hepatol. 26 (2011) 1238–1246.
[18] Z. Jancsó, E. Hegyi, M. Sahin-Tóth, Chymotrypsin reduces the severity of secretagogue-induced pancreatitis in mice, Gastroenterology 155 (2018) 1017–1021.
[19] J. Li, M. Ma, S. Zhang, W. Dong, P. Ma, Z. Zhang, et al., Cholesterol esterase-responsive near-infrared fluorescent probe for precise imaging of atherosclerosis, Sens. Actuators B Chem. 427 (2025) 137150.
[20] A. de Bray, A.G. Roberts, S. Armour, J.S. Tong, C. Huhn, B. Gatin-Fraudet, et al., Fluorescent GLP1R/GIPR dual agonist probes reveal cell targets in the pancreas and brain, Nat. Metab. 7 (2025) 1536–1549.
[21] C. Bastard, C. Caumont, L. Samaison, I. Quintin-Roué, L. Doucet, P. Marcorelles, et al., Fluorescent in situ hybridization testing allows the diagnosis of nrg1 gene fusions in lung and pancreas cancers with no other identified oncogenic driver, Cancers 17 (2025) 2347.
[22] S.A. Bernhard, H. Gutfreund, The optical detection of transients in trypsin- and chymotrypsin-catalyzed reactions, Proc. Natl. Acad. Sci. U. S. A. 53 (1965) 1238–1243.
[23] I. Piovarci, T. Hianik, I.N. Ivanov, Detection of Chymotrypsin by optical and acoustic methods, Biosensors 11 (2021) 63.
[24] H. Shi, C. Liu, J. Cui, J. Cheng, Y. Lin, L. Gao, et al., Perspective on chymotrypsin detection, N. J. Chem. 44 (2020) 20921–20929.
[25] Y. Chen, J. Cao, X. Jiang, Z. Pan, N. Fu, A sensitive ratiometric fluorescence probe for chymotrypsin activity and inhibitor screening, Sens. Actuators B Chem. 273 (2018) 204–210.
[26] A. Endo, T. Kurinomaru, K. Shiraki, Hyperactivation of serine proteases by the hofmeister effect, Mol. Catal. 455 (2018) 32–37.
[27] Y. Qu, Z. Xu, J. Wang, W. Liu, A. Iqbal, K. Iqbal, et al., Strong red fluorescent probe for detecting chymotrypsin activity in vivo and in vitro, Sens. Actuators B Chem. 382 (2023) 133552.
[28] B. Daurai, A.J. Baruah, M. Gogoi, Point-of-care optical device for estimation of α-amylase using carbon quantum dots, IEEE Sens. J. 25 (2025) 16061–16067.

[29] X. He, L. Li, Y. Fang, W. Shi, X. Li, H. Ma, In vivo imaging of leucine aminopeptidase activity in drug-induced liver injury and liver cancer via a near-infrared fluorescent probe, Chem. Sci. 8 (2017) 3479–3483.
[30] Z. Li, P. Huang, G. Wu, W. Lin, Activatable fluorescent probe for studying drug-induced senescence in vitro and in vivo, Anal. Chem. 96 (2024) 12189–12196.
[31] Y. Zhang, X. Chen, Q. Yuan, Y. Bian, M. Li, Y. Wang, et al., Enzyme-activated near-infrared fluorogenic probe with high-efficiency intrahepatic targeting ability for visualization of drug-induced liver injury, Chem. Sci. 12 (2021) 14855–14862.
[32] S. Yamashita, M. Sakabe, T. Ishizawa, K. Hasegawa, Y. Urano, N. Kokudo, Visualization of the leakage of pancreatic juice using a chymotrypsin-activated fluorescent probe, Br. J. Surg. 100 (2013) 1220–1228.
[33] L. Dai, Q. Zhang, Q. Ma, W. Lin, Emerging near infrared fluorophore: dicyanoisophorone-based small-molecule fluorescent probes with large stokes shifts for bioimaging, Coord. Chem. Rev. 489 (2023) 215193.
[34] S. Fan, X.H. Zheng, X.G. Bai, X.W. Guo, H.S. Gao, Z.H. Zhang, et al., Screening of recognition moieties for chymotrypsin-activatable fluorescent probes and application in early diagnosis of pancreatitis, Sens. Actuators B Chem. 448 (2026) 139024.
[35] J.L.M. Mira, A. Quentel, R.K. Patel, D. Keith, M. Sousa, J. Minnier, et al., Early detection of pancreatic cancer by a high-throughput protease-activated nanosensor assay, Sci. Transl. Med. 17 (2025) 3110.
[36] Y. Seki, T. Ishizawa, G. Watanabe, T. Komatsu, A. Nanjo, T. Ueno, et al., Identification of a pancreatic juice-specific fluorescent probe through 411 probes activated by aminopeptidases/proteases or phosphatases/phosphodiesterases, HPB 27 (2025) 150–158.
[37] D. Chen, G. Nie, Y. Dang, W. Liang, W. Li, C. Zhong, Rational design of near-infrared fluorophores with a phenolic D–A type structure and construction of a fluorescent probe for cysteine imaging, N. J. Chem. 45 (2021) 18528–18537.
[38] T. Lu, A comprehensive electron wavefunction analysis toolbox for chemists, Multiwfn, J. Chem. Phys. 161 (2024) 082503.
[39] T. Lu, F. Chen, Multiwfn: a multifunctional wavefunction analyzer, J. Comput. Chem. 33 (2011) 580–592.
[40] O. Trott, A.J. Olson, AutoDock Vina: improving the speed and accuracy of docking with a new scoring function, efficient optimization, and multithreading, J. Comput. Chem. 31 (2009) 455–461.
[41] H. Xiong, R.-R. Li, S.-Y. Liu, F.-X. Wu, W.-C. Yang, G.-F. Yang, Discovery of specific nonpeptide probe for chymotrypsin via molecular docking-based virtual screening and the application, ACS Appl. Bio Mater. 1 (2018) 310–317.
[42] P. Siriviriyakul, T. Chingchit, N. Klaikeaw, M. Chayanupatkul, D. Werawatganon, Effects of curcumin on oxidative stress, inflammation and apoptosis in L-arginine induced acute pancreatitis in mice, Heliyon 5 (2019) e02222.
[43] Q. Yin, W. Yang, Y. Huang, Y. Zhu, J. Ding, B. Li, et al., Near-infrared imaging of acute pancreatitis with a pancreatic lipase-monitoring fluorescence probe, Sens. Actuators B Chem. 414 (2024) 135970.

Wanwei Zhang is currently a master degree student in College of Chemistry, Jilin University. Her interest is spectral analysis.

Mo Ma is currently a Ph.D. student in School of Pharmacy, Jilin University. His interest is spectral analysis.

Chen Zhao is currently a Ph.D. student in College of Chemistry, Jilin University. Her interest is spectral analysis.

Pinyi Ma gained his doctor's degree from College of Chemistry, Jilin University in 2017 and he is an associate professor in that school. His research area is spectral analysis.

Daqian Song gained his doctor's degree from College of Chemistry, Jilin University in 2003 and he is a professor in that school. His research areas are spectral and chromatography analysis.

Ying Sun gained her doctor's degree from College of Chemistry, Jilin University in 2009 and she is a professor in that school. Her research area is spectral analysis.